

Model and simulation of a solar kiln with energy storage

D. Luna^a, J.-P. Nadeau^{a,*}, Y. Jannot^b

^a Arts et Métiers ParisTech, TREFLE CNRS UMR 8508 Esplanade des Arts et Métiers 33405 Talence, France

^b LEMTA UMR CNRS 7563, 2, Avenue de la Forêt de Haye 54504 Vandoeuvre, France

ARTICLE INFO

Article history:

Received 19 February 2009

Received in revised form

22 March 2010

Accepted 22 March 2010

Available online 6 May 2010

Keywords:

Solar kiln

Energy storage

Modeling

Quality

ABSTRACT

A solar kiln with energy storage can be used for continuous drying. This kiln consisted of several units which were modeled to simulate it in operation. A model was proposed for each unit, and another based on laboratory tests for drying a wooden board by passing air across. These models were combined to produce a global model. Simulation results were then analyzed and showed that the use of storage was justified to reduce drying time. Moreover, with the judicious use of storage and air renewal, drying schedules could be produced for a better quality of dried wood.

© 2010 Elsevier Ltd. All rights reserved.

1. Introduction

Solar systems are currently evolving towards integrating energy storage [1], so as to resolve the problems associated with the intermittent nature of solar energy. The aim is to collect and store solar energy during the daytime and extract it when this energy is not available (during the night and on cloudy days).

A solar kiln for drying boards of pine wood was studied, including a unit for storing energy by sensible heat, using water as the storage fluid and air as the heat extraction fluid. The energy storage unit was made up of two components: the exchange-storage unit and the heating unit, a water-based solar collector. The diagram in Fig. 1 shows the arrangement of the different units that make up the kiln and the position of the stack of wood placed inside.

In order to define the optimal design and the optimal operating conditions of the kiln, a global model must be produced from models of each unit and each external environment. Fig. 1 shows the interactions between the different units and variables concerned. The models involved the system's design variables (DeV, they enable to define the unit rigorously) and operating variables (OpV, they enable to carry out the system according to an operating mode). These models will enable us to estimate the criteria specifying the design: drying time t_S and drying quality. Table 1 lists these variables for each unit.

The drying unit is defined according to the dimensions of the stack of wood. The solar air heating unit is defined by the length L and width l of the collector. The storage unit uses water as the storage fluid and air as the heat extraction fluid. It consists of a reservoir of height H_c and diameter D_c . Air is heated through N dimpled vertical tubes assembled in the water reservoir, which have an interior diameter of d_{int} and are arranged in alternate rows of side e_T . The storage unit is connected to a solar water collector defined by its area and its global efficiency supposed constant and equal to 50%. The “meteorology” external environment model concerns the meteorological conditions in the region of Mexico City. The “wood” external environment model enables to calculate the drying rate of a wooden board (with a thickness of 0.027 m) by passing air across, it was obtained by an experimental approach.

After combining these independent models, a simulation of the diurnal and nocturnal functioning of the kiln for two life situations: “kiln without storage” and “kiln with storage” was produced.

The results were then analyzed and from them the use of this type of kiln could be justified, as well as schedules that could be applied to control the quality of the dried product were suggested.

2. Modeling the solar kiln

2.1. External environment model: meteorology

A typical year was estimated using daily temperatures recorded over a 10-year period (1996–2006) at the meteorological station at Mexico City airport [2]. To estimate the density of the solar flow G^* ,

* Corresponding author. Tel.: +33 556845428; fax: +33 556845436.

E-mail address: jean-pierre.nadeau@bordeaux.ensam.fr (J.-P. Nadeau).

Nomenclature		ε	Efficiency
<i>Symbols</i>		τ_r	Renewal rate
		τ_m	Mixture rate
A	Exchange surface, m^2	<i>Indices</i>	
C_p	Specific heat, $J\ kg^{-1}\ ^\circ C^{-1}$	0	Inlet
d	Diameter of tube, m	1	Outlet
D_c	Diameter of storage unit grill, m	a	Air
eT	Transverse spacing between tubes, m	b	Wood
G^*	Density of solar flow, $W\ m^{-2}$	bs	Dry basis
h	Convective exchange coefficient, $W\ m^{-2}\ ^\circ C^{-1}$	cap	Collector
H	Height, m	cr	Critical
HR	Relative humidity, %	E	Exchange – storage unit
k	Global exchange coefficient, $W\ m^{-2}\ ^\circ C^{-1}$	ext	Exterior
L	Length, m	f	Final
l	Width, m	h	Wet
M	Mass, kg	int	Interior
N	Number of tubes (–)	i	Initial
NUT	Number of transfer units (–)	m	Mixture
P	Pressure, Pa	pb	Stack of wood
q	Air mass flow, $kg\ s^{-1}$	r	Renewed air
T	Temperature, K	s	Dry
t	Time, s	sat	Saturation
U	Speed, $m\ s^{-1}$	stk	Storage
V	Volume, m^3	surf	Surface
W	Moisture content, $kg_w\ kg^{-1}_{bs}$	v	Vapor
ΔH	Latent heat, $J\ kg^{-1}$	w	Water
ρ	Density, $kg\ m^{-3}$		

a simulation program was constructed based on the geographical coordinates of the location and the geometrical characteristics of the solar radiation [3].

2.2. External environment model: wood

To represent the drying of a board of pine wood by passing air across, the characteristic drying curve (CDC) method, developed by

Van Meel [4] was used. This consists in expressing the drying speed as a function of a maximal reference drying speed reduced by a function of the mean instantaneous water content.

Several convective drying experiments were carried out using pine wood and different air conditions (Table 2).

Wood samples ($0.120 \times 0.070 \times 0.027$ m) were dried in the drying tunnel at the TREFLE laboratory where temperature (T_a), relative humidity (HR_a) and air speed (U_a) can be regulated and

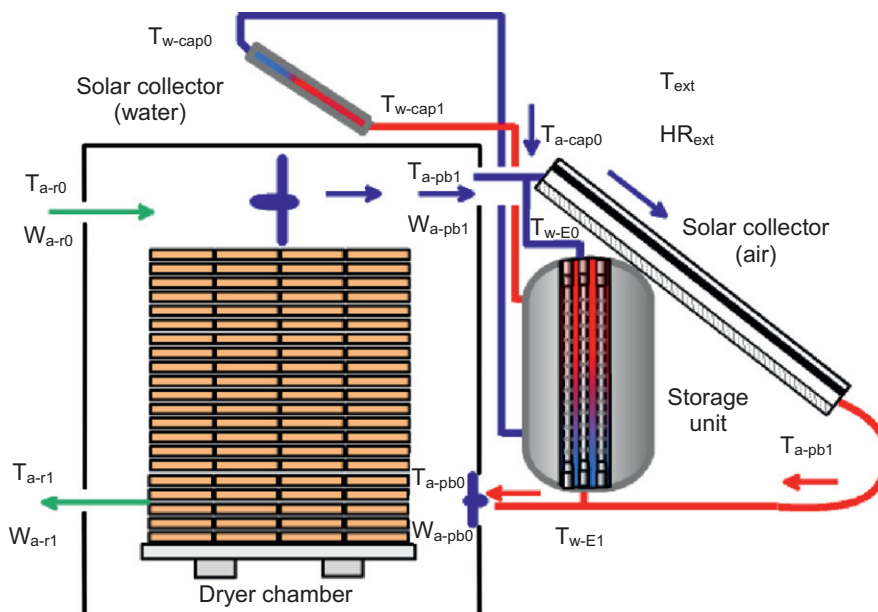


Fig. 1. Solar kiln dryer with energy storage.

Table 1
Design variables associated with each operational unit.

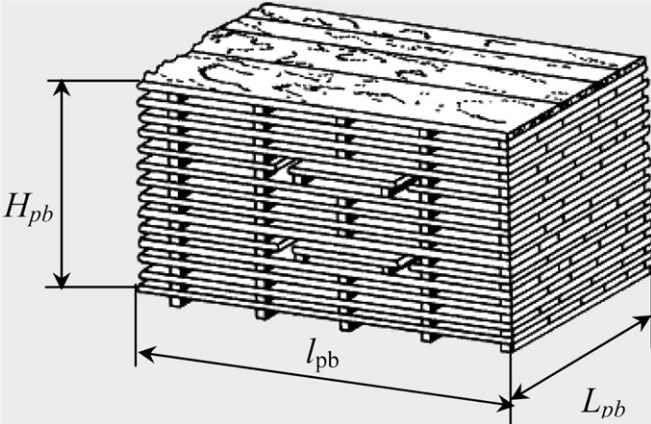

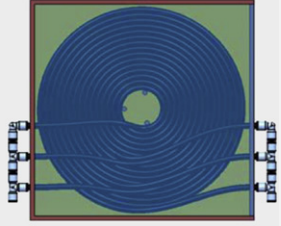
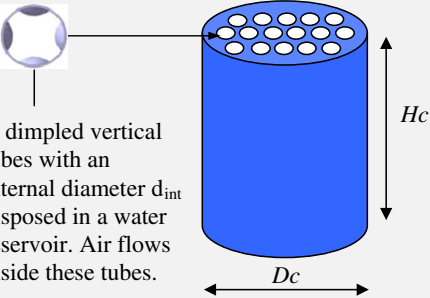
Unit	Figure	DeV	OpV	Cr
Dryer unit		L_{pb}, l_{pb}, H_{pb}	τ_r, τ_m	
Solar air collector		L, l	τ_m	Drying quality, Q Drying time, tS
Solar water collector	<p>$\epsilon_{cap-w} = \phi_u / G * A_{cap-w}$</p> <p>$A_{cap-w} = \pi r^2$</p> 	$A_{cap-w}, \epsilon_{cap-w}$		
Storage unit	 <p>N dimpled vertical tubes with an internal diameter d_{int} disposed in a water reservoir. Air flows inside these tubes.</p>	$H_c, D_c, N, d_{int}, \epsilon_t$		

Table 2
Drying conditions applied in tests.

Test	$T_a, ^\circ C$	$U_a, m\ s^{-1}$	$HR_a, \%$	$T_h, ^\circ C$	$T - T_h, ^\circ C$	$W_{eq}, kg_w/kg_{ss}$	$W_i, kg_w/kg_{ss}$	$W_f, kg_w/kg_{ss}$
1	30	2	50	22	8.0	0.11	0.94	0.12
2	40	2	50	30.3	9.7	0.1	0.8	0.12
3	40	3.5	50	30.3	9.7	0.1	0.76	0.12

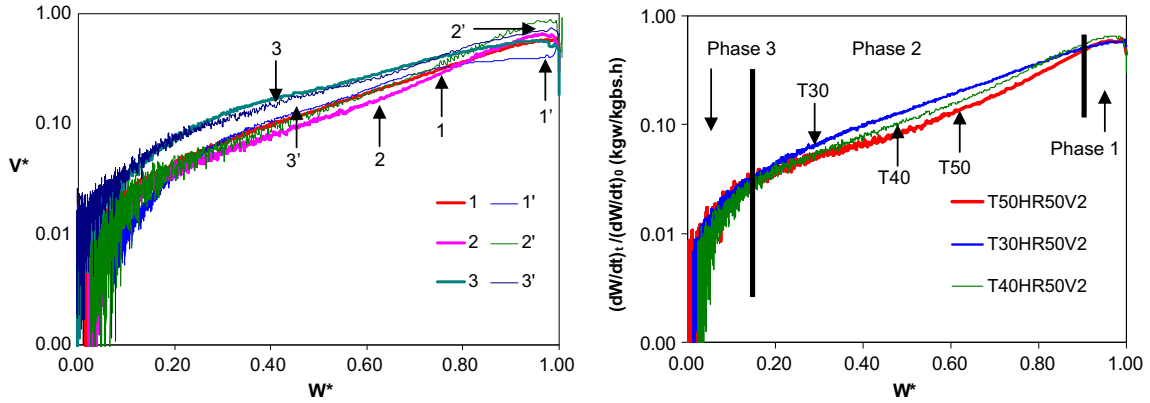


Fig. 2. Experimental drying rate (thickness of plank 0.027 m).

readings for the mass of the sample can be taken continuously. The perimeter of each sample was waterproofed to prevent drying from the sides. A flat product with two faces was considered, where transfers were one-dimensional, in other words, drying by passing air across the sample.

Fig. 2 shows the reduced drying rate as a function of the reduced moisture content W^* for three test groups for different air temperatures with semi-logarithmic coordinates. The samples were such that there was not any free water left on the surface. Phase 1 corresponds to the wood being brought to temperature, phase 2 defines the displacement of the drying front within the board (change in the fiber saturation point of the FSP fibers: $W_{FSP} = 0.33$) and phase 3 indicates that there is not any free water left in the wood board. The reduced drying rate was calculated by dividing the instantaneous drying speed (dW/dt) by the maximal value reached $(dW/dt)_{max}$.

The reduced moisture content is defined as:

$$W^* = \frac{W_b - W_{eq}}{W_{cr} - W_{eq}} \quad (1)$$

where W_b is the mean moisture content of wood, W_{eq} , equilibrium moisture content; W_{cr} , critical moisture content corresponding to the end of the isenthalpic drying phase.

In the specific case of pine wood, the model for a desorption curve found by Lartigue [5] was used. This model, Eq. (2), links the equilibrium moisture content W_{eq} of the wood and the relative humidity HR_a of the air at a given temperature T_a .

$$W_{eq} = \frac{\ln[C - (\ln(HR_a/100)/A)]}{100 \ln(B)} \quad (2)$$

$$A = -2.86 \times 10^{-5} T^2 - 1.07 \times 10^{-2} T + 10.24, B = -5.41 \times 10^{-4} T + 1.01, C = 4.97 \times 10^{-6} T^2 - 2.67 \times 10^{-3} T + 0.35.$$

After analyzing the experimental results, it was possible to write the drying speed in the form:

$$\text{Si } W^* < W_{2-3}^* : \frac{dW_b}{dt} = \left(\frac{dW}{dt}\right)_{max} (cW^* + d) \quad (3)$$

$$\text{Si } W_{2-3}^* < W^* : \frac{dW_b}{dt} = \left(\frac{dW}{dt}\right)_{max} \left[\frac{\exp(bW^*)}{\exp(b)} \right] \quad (4)$$

where the value of W_{2-3}^* corresponding to the transition between drying phases 2 and 3 was estimated at 0.2. This was determined graphically for all the curves with reduced coordinates, (Fig. 2).

The maximal drying speed $(dW/dt)_{max}$ was calculated from a convective type of mass transfer model as a function of the relevant parameters of the drying air ($P_{v-surf}(T_b)$ and P_{v-air}):

$$\left(\frac{dW_b}{dt}\right)_{max} = A [P_{v-surf}(T_b) - P_{v-a}]^\alpha U_a^\beta \quad (5)$$

The coefficients A , α , and β were identified by minimizing the sum of the quadratic deviations between the experimental maximal drying rates and the required model, and the drying speed obtained is expressed:

$$\frac{dW_{pb}}{dt} = 0.07611 [P_{v-surf}(T_{pb}) - P_{v-a}]^{-0.009301} U_a^{0.4099} \left\{ \frac{0.361 W^*}{\exp(3.1446 W^*)} \right\} \quad (6)$$

2.3. Model of the air heating unit

Starting from a complete simulation code for a solar collector, a model was defined which expressed the efficiency of the solar air collector as a function of the design variables L and l , and the

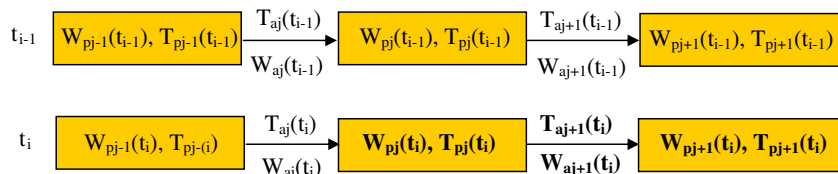


Fig. 3. Principle of the iterative calculation method: known parameters, with parameters to be determined in bold.

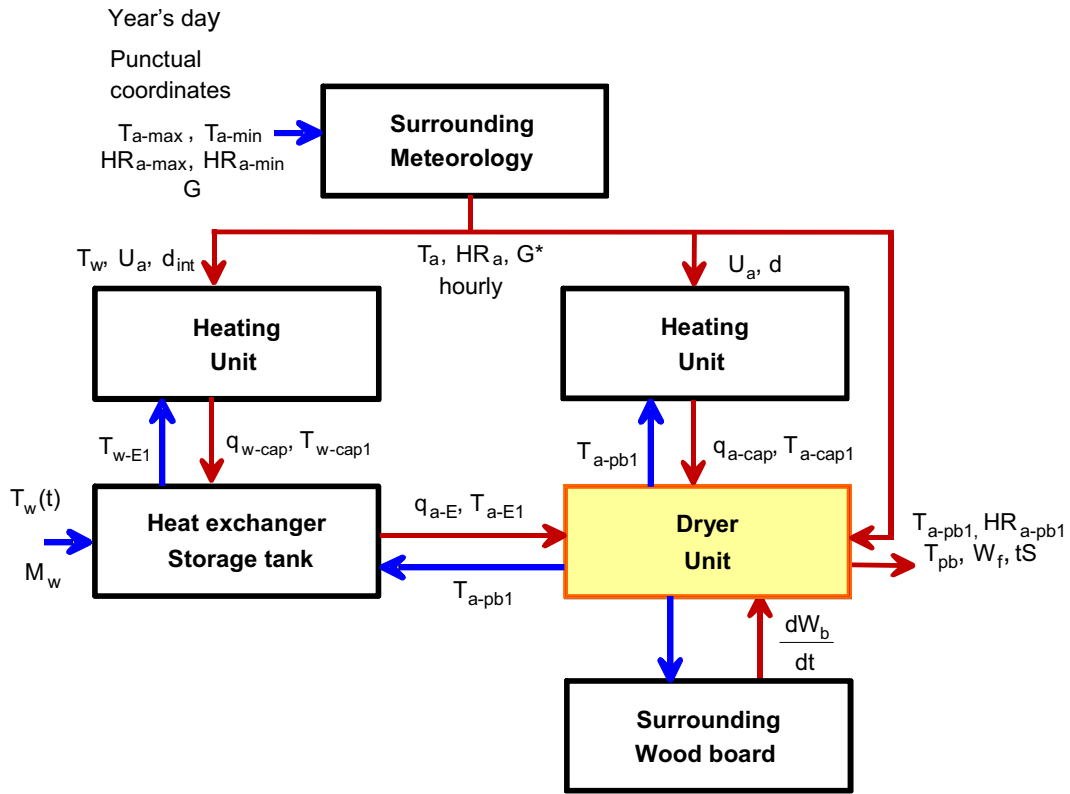


Fig. 4. Diagram of the global model for the solar kiln.

operating variable (τ_m), the rate of mixture in the kiln. The efficiency of the collector is written in the following equation [6]:

$$\epsilon = \frac{\tau_m q_{pb} C_{p_a} (T_{a-cap1} - T_{a-cap0})}{G^* L} = B - K \frac{(T_{a-cap0} - T_{ext})}{G^*} \quad (7)$$

Using a numerical experimental design based on the domains $5 < L < 25$ m and $1.39 < U_a < 4.17$ m/s, efficiency can be expressed as a function of the desired variables [7]:

$$\epsilon = [(0.0037U_a - 0.0254)L + 1.1036 - 0.0134U_a] \times \left[(0.1349 \ln U_a + 0.3163) - (1.3613 \ln U_a + 3.3291) \frac{(T_{a-cap0} - T_{ext})}{G^*} \right] \quad (8)$$

Air speed depends on the width of the collector and the mixture rate.

2.4. Model of the drying unit

The wood boards were stacked one above the other in several layers of n boards in the direction of the air flow with the distance between layers dictated by the thickness of the battens, a (Fig. 3). The hypotheses for modeling the stack of wood were as follows:

- air speed is the same across all the wood boards.
- the mean moisture content $W_{pb}(x, t)$ of a wood board depends only on its position in relation to the air input represented by x and the time t elapsed since the beginning of the drying process.

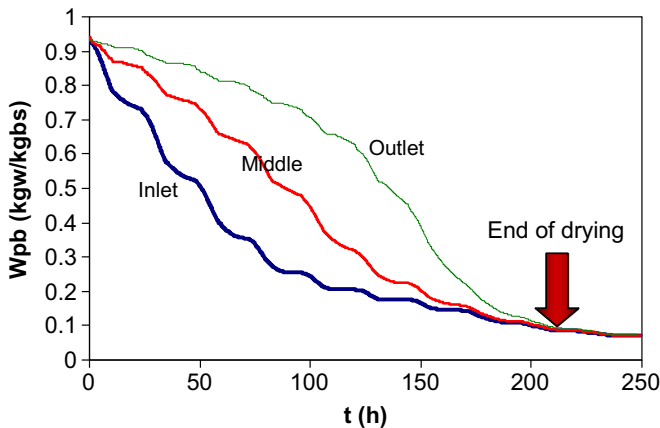


Fig. 5. Water content evolution of the wood during drying.

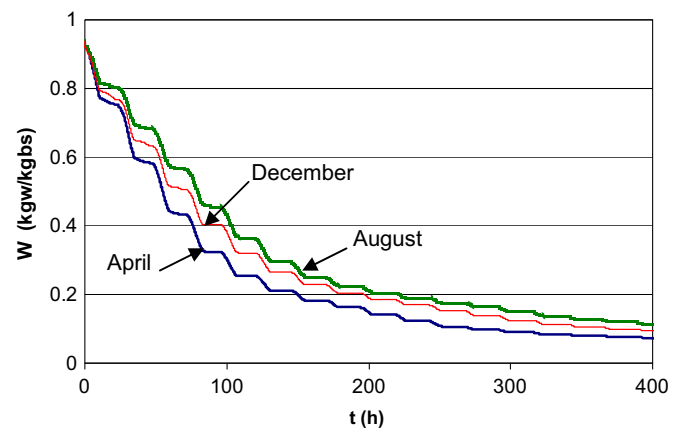


Fig. 6. Seasonal variation in drying rate for stack of wood (without storage).

Table 3
Meteorological conditions for the months considered.

Month	Day of the year	Characteristic	T _{max} (°C)	T _{min} (°C)	HR _{max} (%)	HR _{min} (%)	U _{a-pb} (m s ⁻¹)	τ _r (%)	A _{cap} (m ²)	q _{cap} (kg s ⁻¹)
April	105	Hottest and driest	26	12	70	21	1	30	30	0,5
August	227	Wettest	22	12	81	38				
December	349	Coldest	21	4	85	26				

Given these hypotheses, in order to monitor changes in the conditions of the product and the air at every point in the kiln, the procedure suggested by Jannot [8] was adopted. The following diagram shows the principle used for our calculations.

Thus we calculated:

- the moisture content $W_{pj}(t_i)$ of the j th wood board at instant t_i ,
- the temperature $T_p(t_i)$ of the j th wood board at instant t_i ,
- the air conditions $T_{aj+1}(t_i)$ and $W_{aj+1}(t_i)$ at instant t_i after contact with the j th wood board knowing:
 - the moisture content $W_{pj}(t_{i-1})$ of the j th wood board at instant t_{i-1} ,
 - the temperature $T_p(t_{i-1})$ of the j th wood board at instant t_{i-1} ,
 - the air conditions $T_{aj}(t_i)$ and $W_{aj}(t_i)$ at instant t_i before contact with the j th wood board.

2.5. Mass conservation for wood

From the mass balance for the j th wood board between instants t_{i-1} and t_i , $W_{pj}(t_i)$ could be calculated from:

$$M_j(t_i) = M_j(t_{i-1}) - dM_j(t_i) \quad (9)$$

with

$$dM_j(t_i) = M_{js} \left[-\frac{d\bar{W}_{pj}(t_i)}{dt} \right] (t_i - t_{i-1}) \quad (10)$$

where M_{js} is the dry mass of the j th wood board, invariant with time, and

$$\frac{dW_{pj}(t_i)}{dt} = \left(\frac{dW_{pb}}{dt} \right)_{\max} [U_a, T_{aj}(t_i), HR_j(t_i)] \times f \{ W(t_{i-1}), W_{eq} [T_{aj}(t_i), HR_j(t_i)] \} \quad (11)$$

according to Eq. (8).

2.6. Mass conservation for air

From the mass balance for air it was possible to calculate $W_{pj+1}(t_i)$ from:

$$\rho_a V_a \frac{dW_a}{dt} + \rho_b^s V_b \frac{d\bar{W}_{pb}}{dt} = 0 \quad (12)$$

Volume V_a is the volume swept by the air per unit of time, it is linked with the air flow rate passing through the stack.

Table 4
Result of “seasonal variation” drying schedules.

Month	April	August	December
tS (h) $W_f = 0.12$ kg _w /kg _{bs}	230 h (9.6 d)	302 h (12.6 d)	370 h (15.4 d)

2.7. Energy conservation for wood

$$-hA_j(t_i) [T_{pj}(t_i) - T_{aj}(t_i)] - M_j(t_i) C_p [T_{pj}(t) - T_{pj}(t_{i-1})] - M_{js} \frac{d\bar{W}_j(t_i)}{dt} \Delta H = 0 \quad (13)$$

2.8. Energy conservation for air

Lastly, a heat balance for the air before and after heat and mass exchange with the j th wood board enabled us to calculate $T_{aj+1}(t_i)$:

$$\rho_a V_a (C_{pa} + W_a C_{pw}) \frac{dT_a}{dt} - hA (T_{pb} - T_a) = 0 \quad (14)$$

2.9. Model of the storage unit in extraction life situation

We used the law of energy conservation applied to air:
Hypotheses:

- Water is perfectly mixed, T_w is uniform throughout the storage unit,
- Storage unit is perfectly heat insulated.

$$-M_w C_{pw} \frac{dT_w}{dt} + q_a C_{pa} (T_{a-E1} - T_{a-E0}) = 0 \quad (15)$$

To facilitate the study of this type of system, the adimensional notions of Number of thermal Transfer Units (NUT) and thermal efficiency were introduced, as described by Kays and London [9]:

$$\varepsilon_{a-E} = \frac{(T_w(t) - T_{a-E1})}{(T_w(t) - T_{a-E0})} = 1 - \exp^{-\text{NUT}} \quad (16)$$

$$\text{NUT} = \frac{kA}{q_a C_{pa}} \quad (17)$$

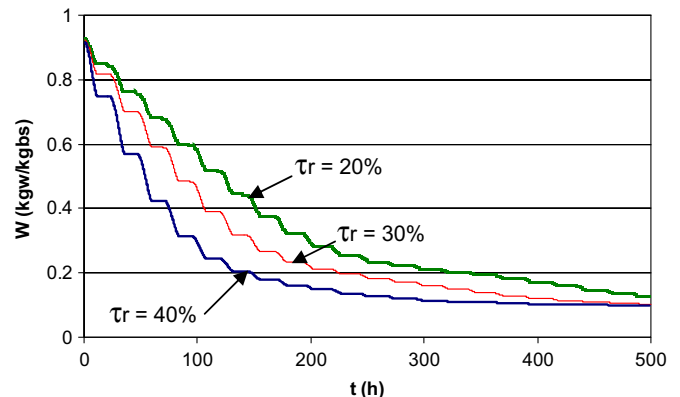


Fig. 7. Influence of τ_r on drying time (month of August).

Table 5
Result of drying schedules based on τ_r rate.

Criteria	τ_r (%)		
	20	30	50
tS (h), $W = 0.12 \text{ kg}_w/\text{kg}_{bs}$	500 h (21 d)	393 h (16 d)	270 h (11 d)

$$A = NH\pi d_{int} \tag{18}$$

Using the global balance (19), the water temperature could then be calculated at every instant by integrating the expression:

$$M_w C_{pw} \frac{dT_w}{dt} = q_a C_{pa} \varepsilon_{a-E} (T_w(t) - T_{a-E0}) \tag{19}$$

$$T_w(t + dt) = T_{a-E0} + (T_w(t) - T_{a-E0}) \exp\left(-\frac{q_a C_{pa} \varepsilon_{a-E} dt}{M_w C_{pw}}\right) \tag{20}$$

With:

$$M_w = \rho H \left(\frac{\pi D c^2}{4} - N \pi d_{ext}^2 \right) \tag{21}$$

If the grill around the tubes has no play in it then the diameter can be calculated as:

$$Dc = 1.25 e_T \sqrt{N} \tag{22}$$

2.10. Global model, interaction between models of the units

The global model of the solar kiln was constructed according to the global diagram shown in Fig. 4.

The interaction flows (mass and energy) between the units brought into play state variables for air, temperature and moisture content, and rate of flow entering each unit. For the drying schedule for the kiln, the operating variables were used and the air mixture rate τ_m and renewal rate τ_r came into play. The mixture rate defines the fraction of flow taken from the kiln to be heated in the air collector by day or in the exchange storage unit by night. The renewal rate defines the fraction of flow that is evacuated and replaced by air from the exterior.

3. Simulation and results

A simulation is presented for a solar kiln in operation for two life situations: operating by day (drying without storage) and operating by night (drying with storage).

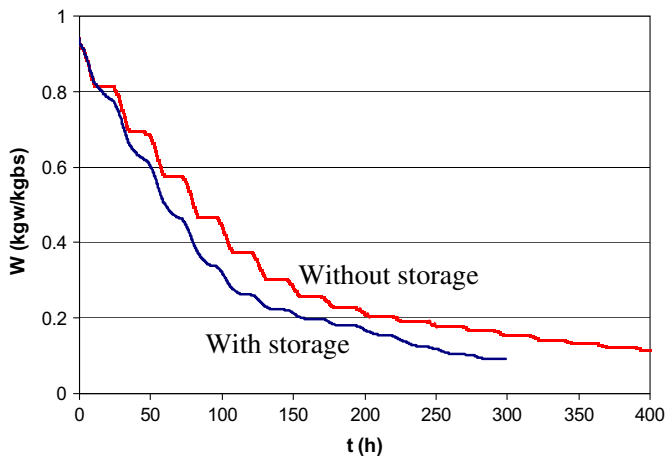


Fig. 8. Influence of energy storage on drying time (month of August).

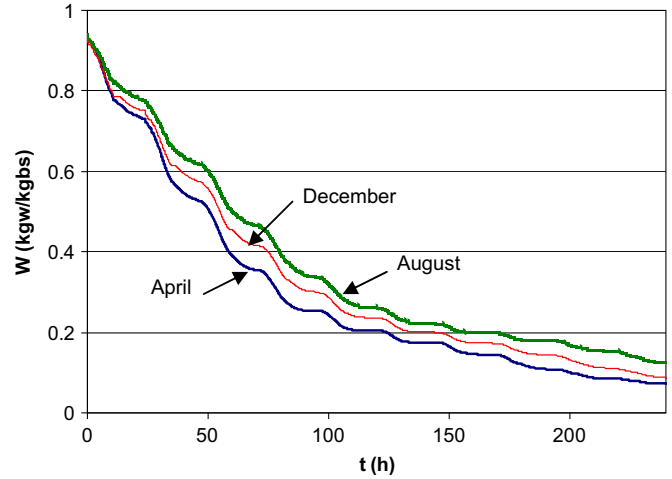


Fig. 9. Seasonal variation in drying time for a stack of wood (with storage).

3.1. Homogeneity and the end of the drying process

Moisture content was analyzed on entry, in the middle and on exit from the stack of wood and showed that there was, of course, a difference in drying depending on where a wood board was located in the pile, however the moisture content for use ($W_f = 0.12 \text{ kg}_w/\text{kg}_{bs}$) was reached within the same time, whatever the position of the board, as shown in Fig. 5.

3.2. Drying without using the storage unit

Fig. 6 gives the drying times for three representative months (considering day 15 of each month). The drying conditions used (relative mean monthly temperature and humidity) are presented in Table 3.

We considered a stack of pine wood with an initial moisture content of 0.94. The dimensions were: $2.16 \times 1.60 \times 2.5 \text{ m}$ with a distance of 0.027 m between layers (battening).

3.3. Seasonal influence

The drying curves shown in Fig. 6 present the same behavior as that observed in the simulation by Khater et al. [10] who used the convective drying model suggested by Nadeau et al. [11]. The difference between daytime and night time drying can be clearly seen.

The strong influence of the relative humidity of the air on drying speed was noted. A faster drying was noted in April (the driest month) than in August (the wettest month), even though temperatures were very similar. In December, drying was faster than in August, even though temperatures were lower. The influence of the humidity of the external air was also observed. Table 4 shows the drying times needed to achieve the required moisture content for use $W_f = 0.12 \text{ kg}_w/\text{kg}_{bs}$.

3.4. Influence of air renewal rate (τ_r)

The air renewal rate τ_r is an operating variable for the kiln from which drying schedules can be established by controlling air humidity. Simulations were carried out for the drying conditions mentioned earlier (Table 3), and a fixed U_{apb} of 1 m/s. Results for August are shown in Fig. 7.

Results showed that the air renewal rate τ_r parameter has a considerable influence on the drying time for the wood. Note in

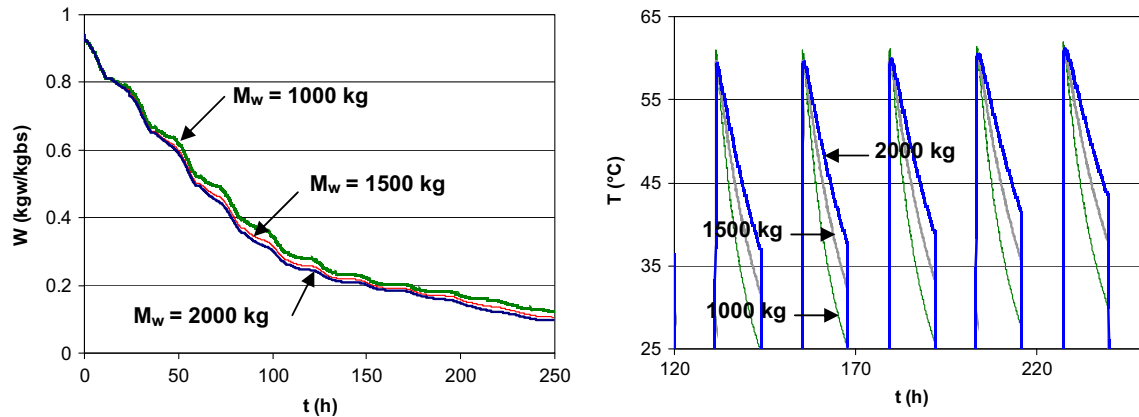


Fig. 10. Influence of mass of storage water M_w on inlet air temperature T_{a-E1} .

Fig. 7 that drying is faster when $\tau_r = 50\%$ than when $\tau_r = 20\%$. This shows a time saving over 50% when considering a final water content of $0.12 \text{ kg}_w/\text{kg}_{bs}$, (Table 5).

4. Drying using the storage unit

4.1. Influence of storage

By integrating an energy storage unit it is possible to carry out drying continuously without interruption. The function of the unit is to store the solar energy during the day and return it when the system needs it. To show the influence that storage can have, two drying simulations (with the same global surface area in both collectors) were compared: one system without storage consisting of an air solar collector measuring 40 m^2 , $U_{a-pb} = 1 \text{ m s}^{-1}$, $\tau_r = 30\%$ and $\tau_{rN} = 5\%$ (renewal rate at night). Another using the storage unit and the following parameters: $A_{cap} = 30 \text{ m}^2$, $A_{capw} = 10 \text{ m}^2$, τ_r and τ_{rN} the same as in the previous case. These results are shown in Fig. 8.

In the case of operating with storage, a mass of water of 1000 kg was considered with an air flow rate in the storage unit of 0.5 kg s^{-1} . The data for operating without storage corresponded to the data given in Table 3.

Fig. 8 shows a considerable reduction in drying time as a result of integrating a storage function when the kiln was operational. The time saving can be as much as 30% for August, considering the moisture content required for use.

4.2. Seasonal influence

Three simulations are presented in Fig. 9 to match the external conditions described in Table 2. We considered the following drying times: $U_a = 1 \text{ m s}^{-1}$, $\tau_{rj} = 30\%$, $\tau_{rN} = 5\%$, $M_w = 1000 \text{ kg}$, $A_{cap} = 30 \text{ m}^2$, $A_{capw} = 10 \text{ m}^2$.

4.3. Influence of the mass of water

The influence of the mass of storage water on the exit temperatures from the exchange unit and on drying times is defined in Fig. 10. The worst drying conditions (August) and the following parameters were taken into account:

$$U_a = 1 \text{ m s}^{-1}, \tau_r = 30\%, \tau_{rN} = 5\%, A_{cap} = 30 \text{ m}^2, A_{capw} = 10 \text{ m}^2.$$

The variation in storage mass parameter has an influence on drying time (Table 6). A one-day time saving was observed when drying with a mass of water $M_w = 2000 \text{ kg}$ instead of $M_w = 1000 \text{ kg}$.

For the exit temperature from the exchange unit (T_{a-E1}), the end of the drying period is the moment where the air temperature was considered to potentially play a more important part. At the 6th day of drying, the exit temperature from the exchange unit was around $12 \text{ }^\circ\text{C}$ higher with a 2000 kg mass of water than when $M_w = 1000 \text{ kg}$.

5. Drying schedule for better quality

5.1. Drying quality

The appearance of a split in the wood is associated with the presence and reversal of stresses within the thickness of the wood [12]. The critical phase occurs when fiber saturation point is reached. To control quality, the drying process was slowed in the $0.25 < W < 0.35 \text{ kg}_w/\text{kg}_{bs}$ stage thus allowing the stresses to relax. To do this, the drying speed is limited. What this limit should be was estimated by considering several experimental kinetics applied to pine wood [11,13]. The calculated drying rate threshold to guarantee quality, was: $dW/dt = 0.01 \text{ kg}_w \text{ kg}^{-1}_{bs} \text{ h}^{-1}$.

5.2. Drying schedules for quality

Once again the operating air renewal variable rate τ_r was used to manage humidity and air temperature conditions inside the kiln and thus control the drying speed.

Two schedules were drawn up in which we succeeded in imposing gentle conditions during the drying process so that the quality threshold was respected. The first involved using the τ_r variable (day and night) and nocturnal extraction (Fig. 11) (beginning at 7 p.m.). At the beginning of the drying process, some stringent conditions were imposed, then between 0.35 and $0.25 \text{ kg}_w/\text{kg}_{bs}$ the imposed quality threshold was respected. This was called the “nocturnal extraction” (Table 7) schedule.

Fig. 9 shows the result of applying this schedule to two representative months (April and August).

The simulations were carried out with: $A_{cap-a} = 30 \text{ m}^2$, $A_{cap-w} = 10 \text{ m}^2$, $M_w = 1000 \text{ kg}$ and $U_{a-pb} = 1 \text{ m s}^{-1}$.

Table 6
Drying time according to season of the year.

Criteria	April	August	December
tS with storage (h)	180 (8 d)	240 (10 d)	205 (9 d)
$W_f = 0.12 \text{ kg}_w/\text{kg}_{bs}$			
tS without storage (h)	230 h (9.6 d)	302 h (12.6 d)	370 h (15.4 d)
$W_f = 0.12 \text{ kg}_w/\text{kg}_{bs}$			

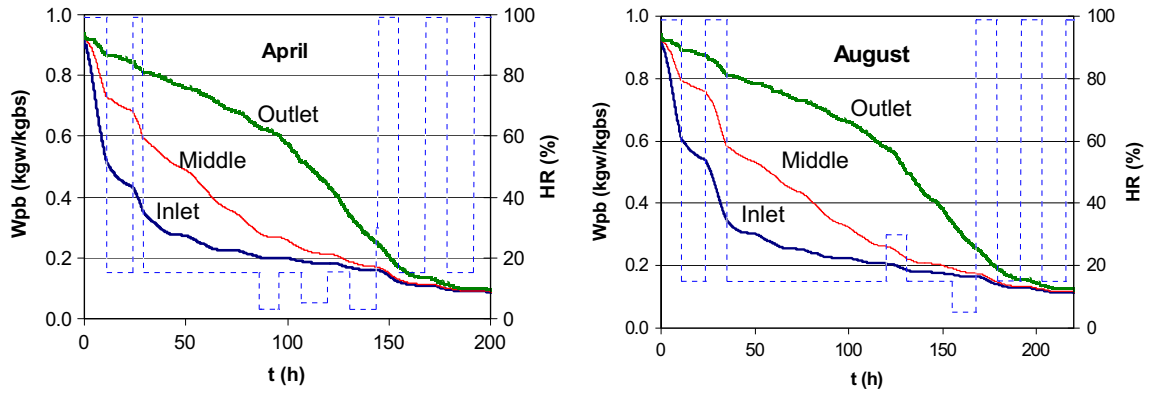


Fig. 11. Simulation of solar drying, taking drying quality into account (nocturnal extraction).

Table 7
"Nocturnal extraction" drying schedule.

$W_{pb}=0.35$	$W_{pb}=0.25$
$\tau_r = 80 \text{ à } 100 \%$	$\tau_r = 15 \%$
Nocturnal extraction 19h to 8h	Nocturnal extraction 19h to 8h, according as $\frac{dW_{pb}}{dt}$
	$\tau_r = 80 \text{ à } 100 \%$
	Nocturnal extraction 19h to 8h

The drying table enabled us to favor quality over length of drying time. This time can be shortened if extraction is begun at 3 p.m. (Fig. 12), as soon as the recovered solar power begins to drop.

In this case (Fig. 10), the air renewal rate was noted to remain virtually constant when passing through the critical moisture content range ($0.35 < W_{pb} < 0.25 \text{ kgw/kgbs}$).

Daily extraction was used at the beginning and at the end of drying during this period and rapid drying was observed. The slowing down of the drying process for the first wood boards extended the drying time. To resolve this, varying the air flow rate in the exchange unit was suggested in order to control the conditions of the air and, at the same time, the running of the schedule through τ_r and extraction.

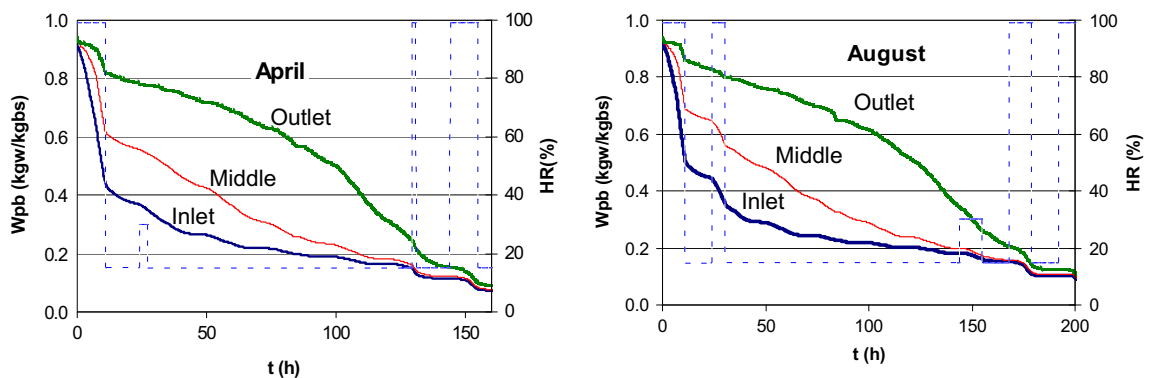


Fig. 12. Simulation of solar drying, taking drying quality into account (extraction at 3 p.m.).

6. Conclusion

A solar kiln for stacks of pine boards which incorporates energy storage can continue the drying process day and night. It consists of a drying unit, an air heating unit and a storage unit for energy by sensible heat. In order to calibrate its optimal size and assess its possibilities, models had to be produced for every unit.

The different models were constructed and linked by state variables and air flow rates to produce the global model for the kiln. Models of the external environments were also produced. Trials were carried out in the laboratory for drying wooden boards, resulting in a model which could then be integrated into the global model.

The different simulations showed that there were advantages in energy storage for several reasons. First, up to 30 % of drying time could be saved in August in the Mexico City region. Second, using extraction according to carefully prepared drying schedules, the quality of the finished product can be controlled without increasing the drying time.

References

- [1] Luna D, Nadeau JP, Jannot Y. Solar timber kilns: State of the art and foreseeable developments. *Renewable & Sustainable Energy Reviews*; 2008.
- [2] www.espanol.wunderground.com (Meteorological data).
- [3] Jannot Y. Thermique solaire. Available from: <http://www.thermique55.com/principal/thermiquesolaire.pdf>; 2008.
- [4] Van Meel DA. Adiabatic conversion batch drying with recirculation of a chemical. *Engineering Science* 1958;9:36–44.
- [5] Lartigue C. Mécanismes élémentaires mis en jeu lors du séchage du pin maritime. Thèse Université de Bordeaux I; 1987.
- [6] Bernard J. Génie Energétique, Energie Solaire: Calculs et optimisation. Ellipses; 2004.
- [7] Luna D, Jannot Y, Nadeau J-P. Parsimonious model of a solar air heater. *Applied Thermal Engineering* submitted for publication.
- [8] Jannot Y. Du séchage des produits alimentaires tropicaux à la caractérisation thermophysique des solides, HDR. Université de Bordeaux I; 2006.
- [9] Kays WM, London AL. Compact heat exchangers. London: MacGrawHill; 1984.
- [10] Khater HK, Helwa NH, Enayet MM, Hashish MI. Optimization of kiln for drying wood. *Drying Technology* 2004;22(4):677–701.
- [11] Nadeau J-P, Puiggali J-R. Séchage, des processus physiques aux procédés industriels. Paris, France: Lavoisier Tec & Doc; 1995.
- [12] Puiggali JR, Nadeau J-P, Sales C. Assessment of timber drying schedules by evaluation of damage risk. *Drying Technology* 1993;11(3):507–24.
- [13] Collignan A, Nadeau J-P, Puiggali JR. Description and analysis of timber drying kinetics. *Drying Technology* 1993;11(3):489–506.